2.7 SOLID-STATE MIXING OF ODS 14YWT AND 9Cr F/M STEEL ALONG BUTT JOINT BY FRICTION STIR WELDING -

D.T. Hoelzer, L. Tan, W. Tang and Z. Feng (Oak Ridge National Laboratory)

OBJECTIVE

The objective of this task is to characterize the solid-state mixing behavior between dissimilar metal joining of the advanced oxide dispersion strengthened (ODS) 14YWT ferritic alloy and reduced-activation 9Cr ferritic/martensitic steel (FMS) along a varying angle butt joint produced by friction stir welding (FSW). The study focuses on understanding the stability of the dispersion-strengthened phases and grain structure in the weld zone and ultimately the quality of the joint between dissimilar metals as a function of FSW process conditions.

SUMMARY

Plates of 5 mm thickness were fabricated from the ODS 14YWT ferritic alloy and 9Cr ferritic/martensitic steel (FMS) and joined by FSW along an effective angle of 9.6º relative to the butt joint between the two plates. Three cross section samples were cut from the joined plates representing solid-state mixtures of ~80%/20%, ~50%/50% and ~20%/80% by volume fraction of 14YWT and 9Cr FMS, respectively and prepared by metallographic procedures. The microstructural analysis of the stir zone observed by Secondary Electron Microscopy (SEM) in the 3 samples showed that very high temperatures from frictional heat caused grain size and oxide particle size increases for 14YWT and decreases in prior austenite grain size and martensite lath size with dissolution of carbides for 9Cr FMS. Complete solid-state mixing occurred in stir zone of the ~50%/50% sample, but only occurred in the region near the pin tool shoulder of the ~80%/20% and ~20%/80% samples.

PROGRESS AND STATUS

Introduction

Friction stir welding (FSW) was previously investigated for joining 14YWT (similar metal) and 14YWT to F82H (dissimilar metal) [1]. In the initial study, the 14YWT specimens were joined along a butt joint while specimens of 14YWT and F82H were joined along a plunge joint. In joining technology, the plunge joint is not as technologically important as is the butt joint. For example, the joining of two pipes is done using a butt joint. However, there have been few studies on the butt joining of dissimilar alloys, especially high strength steels and ferritic alloys, by FSW. This project addresses this deficiency in joining technology and will greatly add to the understanding of solid state mixing of dispersion strengthened dissimilar alloys, such as 14YWT and 9Cr FMS, along a butt joint by FSW. The results of this study will be important for advancing dispersion strengthened ferritic alloys for fusion energy reactors.

Experimental Procedure

Plate samples of 14YWT (SM13 heat) and 9Cr FMS were prepared for the FSW experiment. The SM13 heat of 14YWT was produced and fabricated into 1.06 cm thick plate by cross rolling in the Fuel Cycle Research and Development (FCRD), Nuclear Energy (NE) program. For the FSW experiment, the 1.06 cm thick plate of 14YWT was cross-rolled an addition 53% reduction in thickness at 1000ºC, or 0.5 cm thickness. The dimension of the 14YWT plate was 13.9 cm x 7.5 cm x 0.5 cm thick. The 9Cr FMS was supplied in the final thermo-mechanical treatment (TMT) condition as a 1 cm thick plate, which was mechanically cut along the mid-section of the thickness to 0.5 cm thickness. The final dimension of the plate was 12.7 cm x 5.6 cm x 0.5 cm thick. The plates of 14YWT and 9Cr FMS were cut into two sections with an angle of 7.4º parallel to the longest length. The 7.4º taper angle was based on a pin tool design that ultimately was not used in this experiment. A digital image showing the two plates of 14YWT and 9Cr FMS butted together along the 7.4º angle is shown in Figure 1.

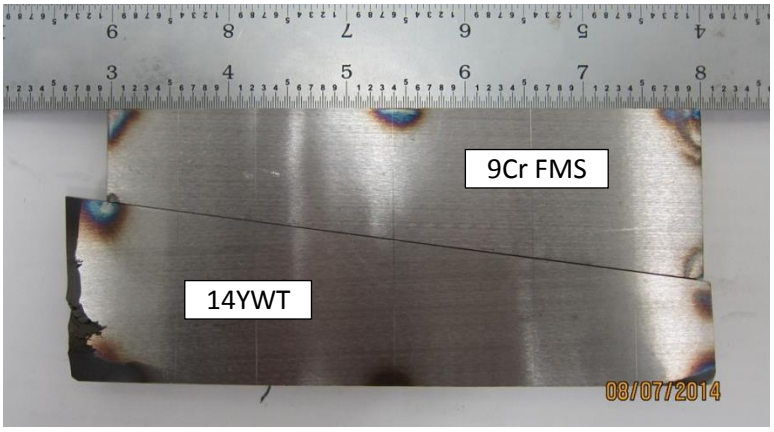

Figure 1. Digital image showing the plates of 14YWT and 9Cr FMS fitted together along the varying angle butt joint.

Figure 2 shows the experimental procedure for joining plates of 14YWT and 9Cr FMS along the varying angle butt joint. The FSW experiment was performed by having the pin tool travel along the center of the two adjacent plates resulting in varying volume fractions of the adjacent dissimilar alloys along the butt joint. Near the beginning, the pin tool will lie mostly in the 14YWT plate and overlap slightly with the 9Cr F/M steel plate to produce ~80%/20% mixture of the 14YWT and 9Cr F/M steel, respectively at the joint. At the mid-point, the pin tool will have roughly the same amount of each plate in the mixture, or 50% 14YWT and 50% 9Cr F/M steel occupying the butt joint. Finally, near the end of the FSW experiment, the pin tool reverses the mixture of the butt joint so that it will include ~20% 14YWT and 80% 9Cr F/M steel

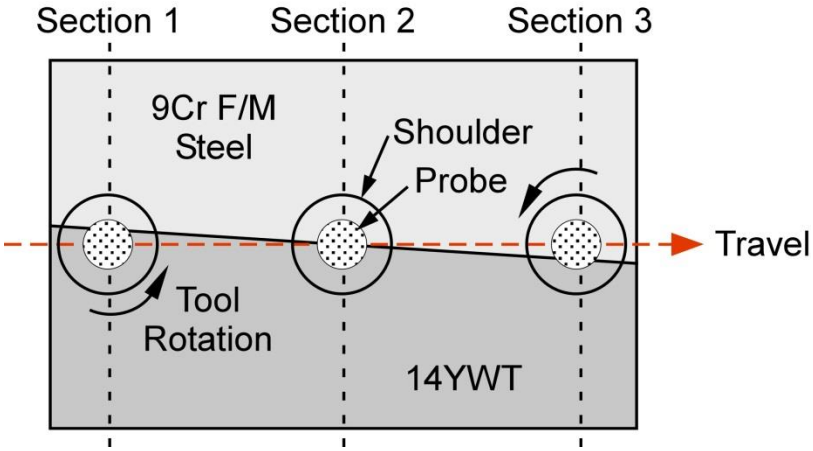

Figure 2. Illustration of the FSW experiment for joining plates of 14YWT and 9Cr FMS along the varying angle butt joint.

The FSW experiment was performed using a Polycrystalline Cubic Boron Nitride (PCBN) pin tool that was 6.5 mm long and tapered from 10 mm dia. at the base of the 25 mm dia. shoulder to 3.5 mm dia. at the tip. Because the dimensions of this pin tool were different from the one used in determining the 7.4º taper angle on the two plates, the path that the pin tool made was increased by 2.2º relative to the taper angle, which meant that the effective angle that the pin tool traveled was 9.6º. This modification was done in order to ensure that the pin tool started completely in the 14YWT plate and ended completely in the 9Cr FMS plate. The FSW run was performed with tool rotation speed of 250 rpm and translation welding speed of 7.62 cm per minute. Cross section samples for microstructural characterization were extracted from three sections of the joined plates illustrated in Figure 2 and were mounted and polished by

metallographic procedures. The final polishing step was conducted using colloidal silica. The microstructural analysis of the FSW samples was investigated using the JEOL 6500 FEG (Field Emission Gun) Scanning Electron Microscope (SEM).

Results and Discussion

Friction Stir Welding Run

The parameters used in the FSW run resulted in the successful joining of the 14YWT and 9Cr FMS plates as shown in Figure 3. The counter-clockwise rotating pin tool first entered the 14YWT plate on the left side of the image and traveled to the right side forming the varying angle butt joint where it exited (concentric rings) from the 9Cr FMS plate. The ascending side of the joined plates mainly contained the 14YWT plate (bottom) while the descending side mainly contained the 9Cr FMS plate (top). The cross section samples prepared for microstructural characterization were cut from the three sections marked with dashed lines and labelled (1A, 2A and 3A) shown in Figure 3.

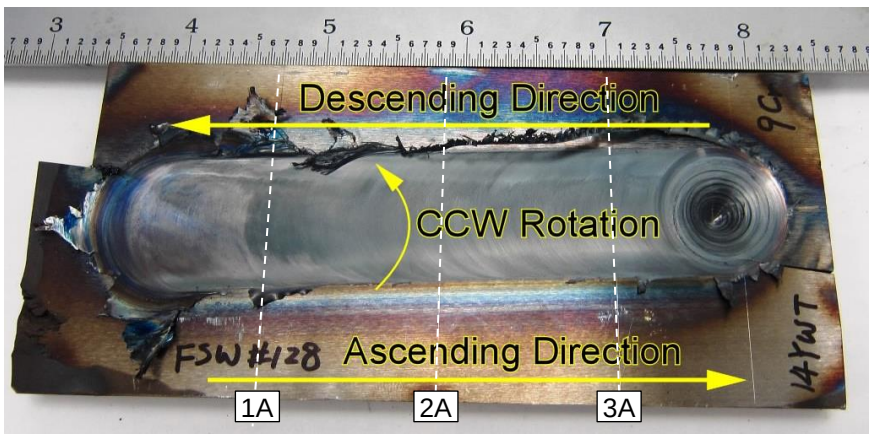

Figure 3. Digital image showing the successfully joined plates of 14YWT and 9Cr F/M steel by FSW along the varying angle joint. The ascending, descending and rotation directions of the pin tool are shown. The ruler shown at the top is in decimal inches.

Microstructural Characterization

The general microstructural features observed with backscattered electron (BSE) imaging for the 3 sample locations on the ascending and descending sides of the joined 14YWT and 9Cr FMS plates are shown in Figures 4 and 5, respectively. All of the BSE micrographs show the microstructure near the joint between the stir zone (SZ), thermomechanically affected zone (TMAZ) and the bottom supporting 9Cr FMS plate.

On the ascending side, the SZ at the 1A and 2 A locations (Fig.'s 4a and 4b) consisted of 14YWT with multiple protrusions extending downward into the supporting 9Cr FMS plate and a clear demarcation in contrast along the interface between the SZ and TMAZ of 14YWT. The finger-like pattern associated with the multiple protrusions of 14YWT into the 9Cr FMS result from the time elapsed behavior of solid-state mixing that occurs as the pin tool travels along the varying angle butt joint. The finger-like pattern suggests that large volume sections of 14YWT and 9Cr FMS must detach and then flow in spiral motion and are then forged in alternating sections as the pin tool progresses in travel. At the 3A location (Fig. 4c) on the ascending side, the SZ consisted of 9Cr FMS with little contrast variation along the interface between the SZ and TMAZ. The vertical crack demarcates the gap between the butted plates of 14WYT and 9Cr FMS that were not joined by the pin tool during the FSW run.

On the descending side, the SZ at the 1A location (Fig. 5a) consists of 14YWT and the interface separating the SZ and TMAZ is barely discernable based on contrast. In addition, the vertical crack observed in this figure defines the gap between the butted plates of 14YWT and 9Cr FMS that were not joined together during the FSW run and the horizontal gap separating 14YWT and 9Cr FMS defines the extent of the TMAZ for 14YWT. Material associated with the horizontal gap region does not experience

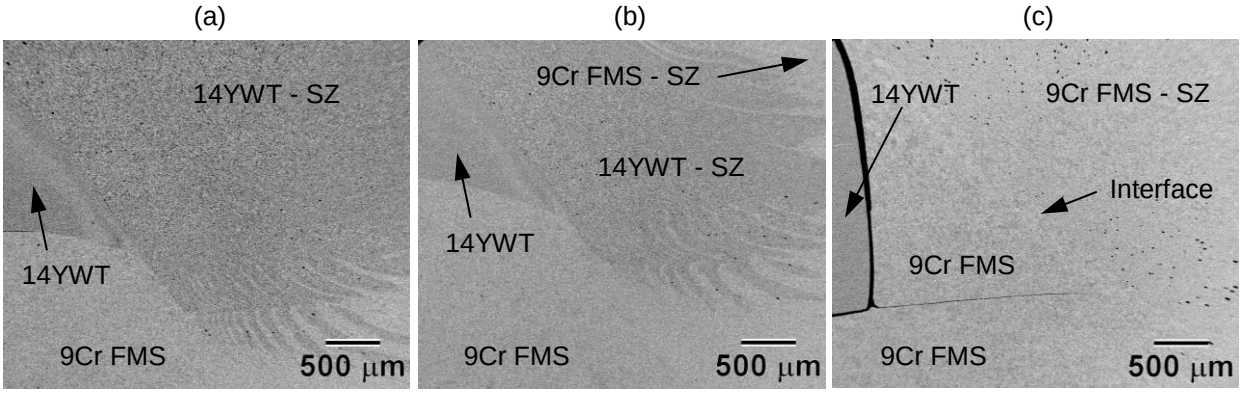

Figure 4. BSE micrographs at very low magnification showing the microstructure on the ascending side of joined plates between 14YWT and 9Cr FMS near the (a) start at 1A, (b) middle at 2A and (c) end at 3A).

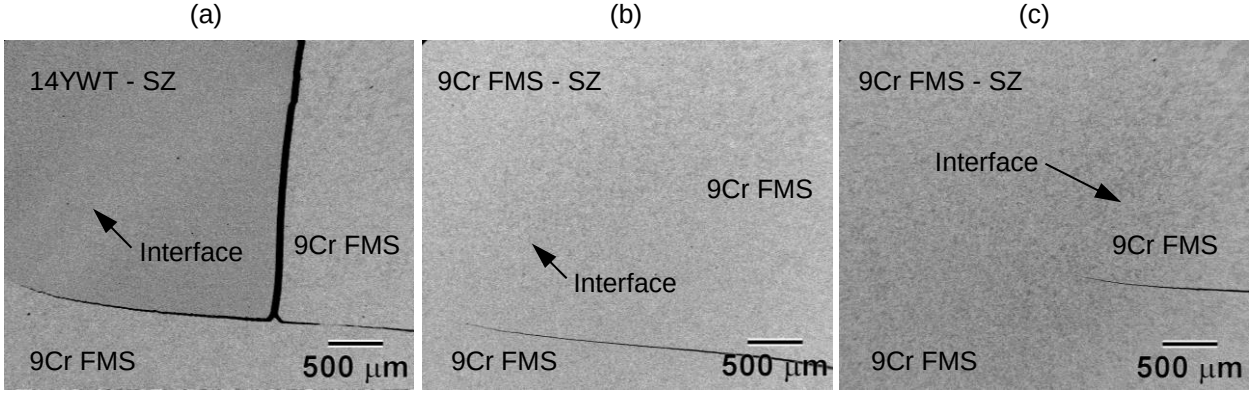

Figure 5. BSE micrographs at very low magnification showing the microstructure on the descending side of joined plates between 14YWT and 9Cr FMS near the (a) start at 1A, (b) middle at 2A and (c) end at 3A).

high enough temperatures during FSW to cause plastic flow. At the 2A and 3A locations (Fig.'s 5b and 5c), the SZ consists of 9Cr FMS with no discernable contrast along the interface between the SZ and TMAZ. However, the extent of the TMAZ can be determined from the end of the horizontal cracks that are due to the gap between the top and bottom plates of 9Cr FMS.

From these results, it was concluded that the microstructure of the SZ at the 2A location (Fig. 4b and 5b) consisted of a mixture of 14YWT and 9Cr FMS. However, due to the location of the 1A and 3A samples relative to the varying angle of the butt joint, little mixing occurred between 14YWT and 9Cr FMS since the microstructure of the SZ consisted almost entirely of 14YWT at the 1A location (Fig.'s 4a and 5a) and mostly of 9Cr FMS at the 3A location (Fig.'s 4c and 5c).

Near the top surface of the joined 14YWT and 9Cr FMS plates, the solid-state mixing behavior in the SZ was influenced by additional heat generated from the rotating shoulder of the pin tool. The microstructure observed with BSE on the ascending and descending sides of sample 1A are shown in Figure 6. On the

ascending side (Fig. 6a), variations in contrast are observed for 14YWT along the interface separating the SZ and TMAZ as well as for different regions of 14YWT in the SZ. The reason for these contrast variations will be shown in following figures. A small section of 9Cr FMS is observed at the top of the sample, which indicated that extensive plastic flow occurred due to the rotating shoulder of the pin tool. This section of 9Cr FMS is also observed at the top of sample 1A on the descending side (Fig. 6b). This result is ascertained by the contrast differences along the interface between the SZ of 14YWT and 9Cr FMS. However, the interface between the SZ and TMAZ of 9Cr FMS is not clearly observed.

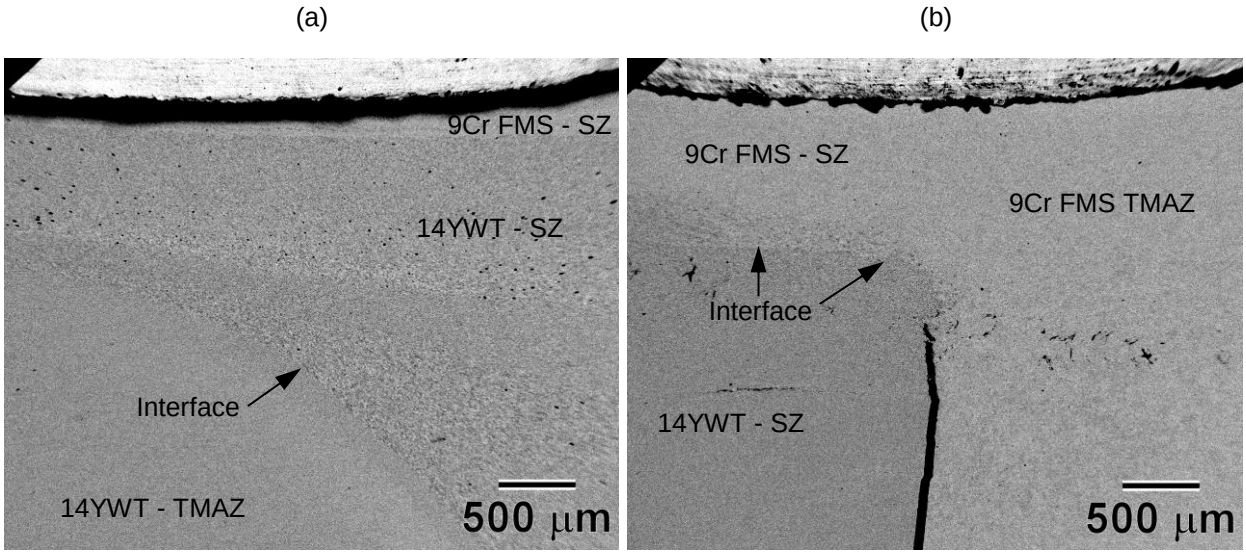

Figure 6. BSE micrographs showing the microstructure observed near the top of sample 1A on: (a) the ascending side and (b) the descending side.

To understand the reasons for the contrast variations observed between different regions of the joint between 14YWT and 9Cr FMS, it is necessary to become familiar with the microstructure observed in the base sections of the 14YWT and 9Cr FMS plates. Figure 7 shows BSE micrographs of the microstructure observed for 9Cr FMS in the unaffected region of the plate, away from the SZ, TMAZ and HAZ. The microstructure consisted of large prior austenite grains containing martensite laths laying in several crystallographic orientations (Fig. 7a) with visible carbides decorating the lath boundaries (Fig. 7b). The carbides show bright contrast relative to the laths indicating that they are composed of elements with high atomic number (Z). The contrast variations observed within the laths are most likely due to backscattered electron channeling variations due to overlapping laths. The typical dimension of the laths are ~1 to 2 μm wide and up to ~10 to 12 μm long. Figure 8 shows BSE micrographs of the microstructure observed for 14YWT in the unaffected region. The microstructure observed at low magnification (Fig. 8a) is noisy due to insufficient resolution for observing the grains. With improved resolution at higher magnification (Fig. 8b), ultra-small grains are observed that are elongated in the horizontal direction, which is parallel to the extrusion direction. Qualitative estimates indicate that the grain size in the unaffected zone is less than ~0.5 μm normal to the extrusion direction and up to ~2-3 μm parallel to the extrusion direction. The enhanced grain aspect ratio observed for 14YWT was caused by cross rolling the plate to 50% reduction-in-thickness, which compressed the grains in the thickness direction. Also observed at higher resolution are numerous sub-micron size particles and a few sub-micron size pores that show dark contrast in the BSE micrograph compared to surrounding grains. Previous characterization studies of 14YWT revealed that particles larger than ~20 nm were consistent with Ti(C,N) [2], which would account for the dark contrast observed in the BSE micrograph.

The interface region observed between the SZ and TMAZ of 9Cr FMS on the ascending and descending sides of sample 3A is shown in Figure 9. In both micrographs, the microstructure in the SZ appears featureless at low magnifications, while the TMAZ shows contrast variations associated with martensite laths. Numerous sub-micron size spots with dark contrast are distributed in the SZ on the ascending side (Fig. 9a) but are not so prevalent on the descending side (Fig. 9b).

(a) (b)

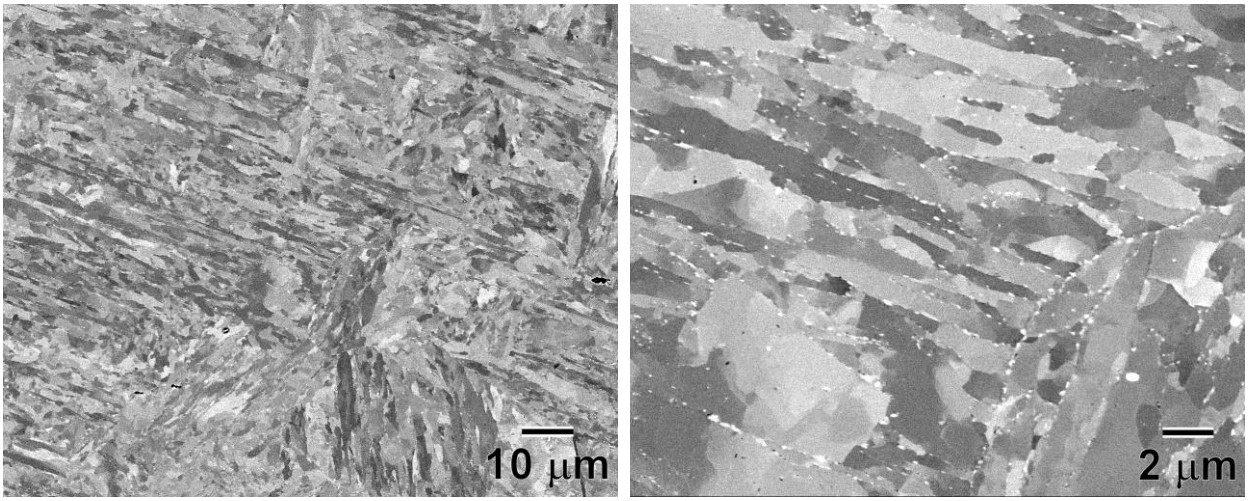

Figure 7. The microstructure observed in the base 9Cr FMS plate away from the SZ, TMAZ and HAZ in sample 3A. (a) BSE micrograph at low magnification and (b) BSE micrograph at higher magnification.

(a) (b)

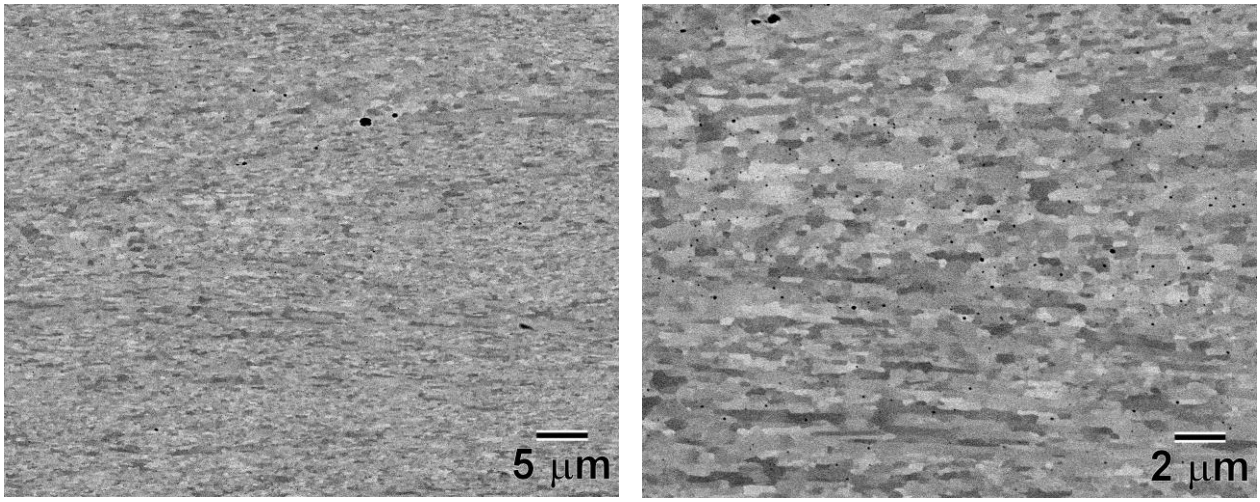

Figure 8. The microstructure observed in the base 14YWT plate away from the SZ, TMAZ and HAZ in sample 1A. (a) BSE micrograph at low magnification and (b) BSE micrograph at higher magnification.

Figure 10 shows BSE and SE (secondary electron) micrographs of the SZ of 9Cr FMS on the ascending side of sample 3A at higher magnification. The results indicated that considerable refinement occurred in the prior austenite grains containing martensite laths (observed in the unaffected zone) in the SZ. The austenite grain boundaries and lath structure are not discernable and no carbide particles are visible. However, there is a one-to-one correlation between the small dark contrast spots observed in the BSE micrograph (Fig. 10a) and the small dark contrast spots observed in the SE micrograph (Fig. 10b). Since

secondary electrons are generated from a depth less than ~10 nm from the surface of the specimen, the contrast, or emission yield, depends mainly on the specimen tilt angle and topography of the specimen surface. Therefore, the white contrast associated with the dark spots observed in the SE micrograph (Fig. 10b) is caused by curvature in the surface topography near the spots, which indicates that most of the dark spots observed on the ascending side of 9Cr FMS are pores.

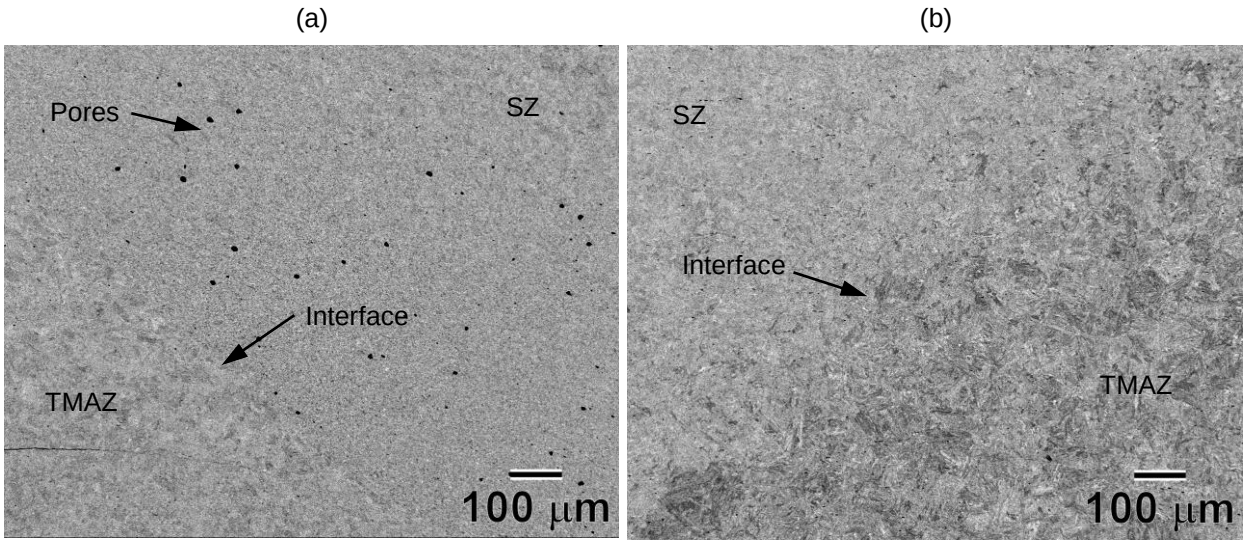

Figure 9. BSE micrographs showing the interface between the SZ and TMAZ of 9Cr FMS in sample 3A on (a) the ascending side and (b) the descending side.

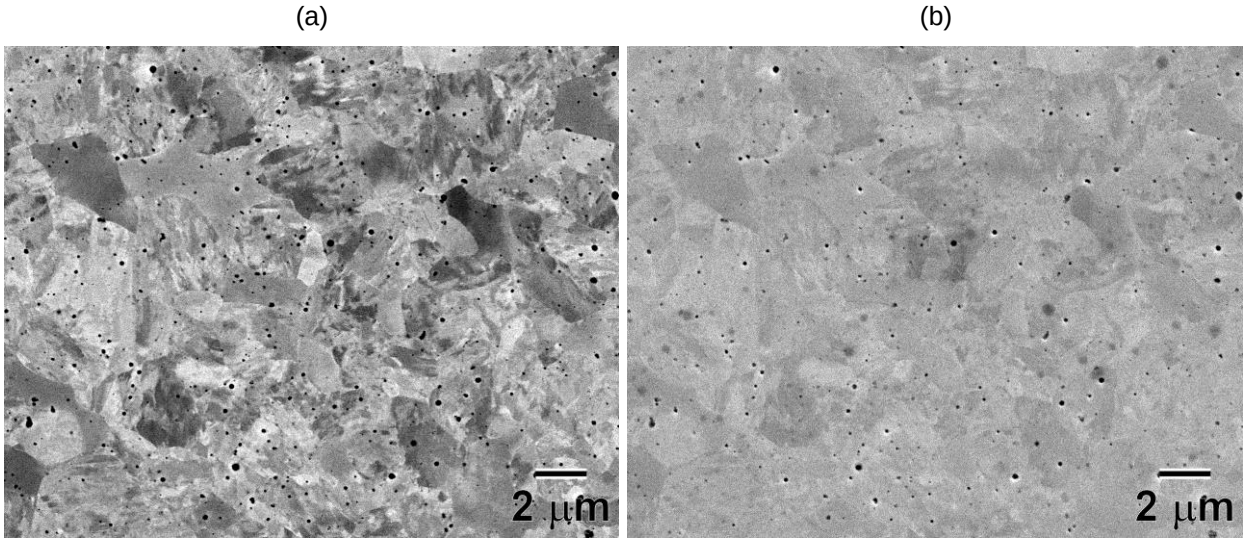

Figure 10. The microstructure observed in the SZ of 9Cr FMS in sample 3A on the ascending side. (a) BSE micrograph and (b) SE micrograph.

The microstructure observed at higher magnification in the SZ of 9Cr FMS on the descending side of sample 3A is shown in Figure 11. Similar to that observed on the ascending side, the austenite grain boundaries and lath structure are not well defined and no carbide particles are visible. A lower population of pores is distributed in the microstructure on the descending side (Fig. 11b) that appear smaller in size compared to those observed on the ascending side (Fig. 10a).

Figure 12 shows the microstructure that was observed at higher magnification in the TMAZ of 9Cr FMS on the ascending and descending sides in sample 3A. On both sides, grain boundaries associated with austenite grains containing martensitic laths showing distinct crystallographic orientations are observed. However, both the austenite grain size and martensite laths have been refined in size compared to the unaffected zone (Fig. 7). A few small particles showing bright contrast can be observed in the TMAZ on

(a) (b)

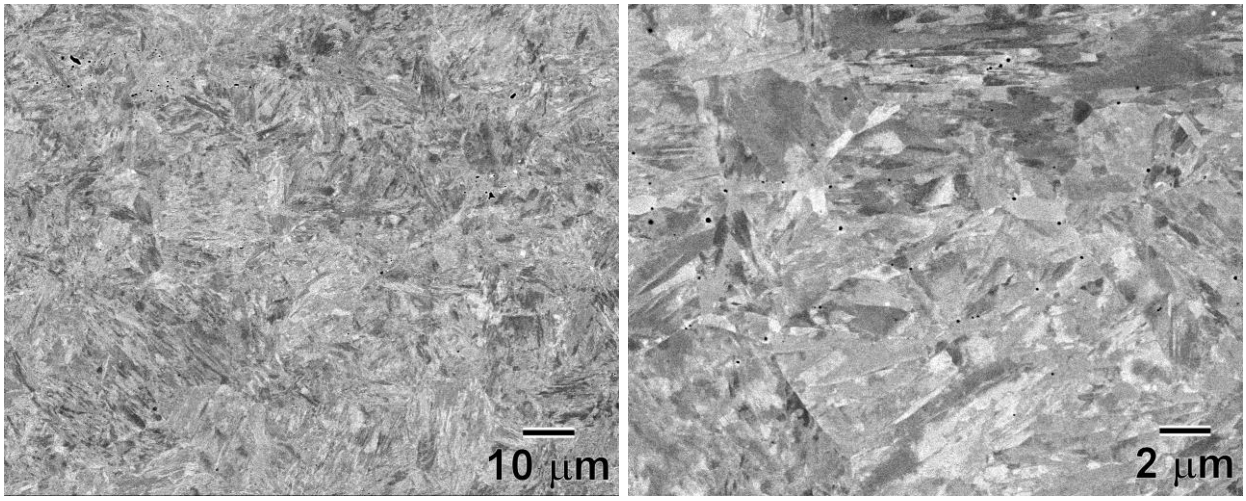

Figure 11. BSE micrographs showing the microstructure observed in the SZ of 9Cr FMS in sample 3A on the descending side. (a) Low magnification and (b) high magnification.

(a) (b)

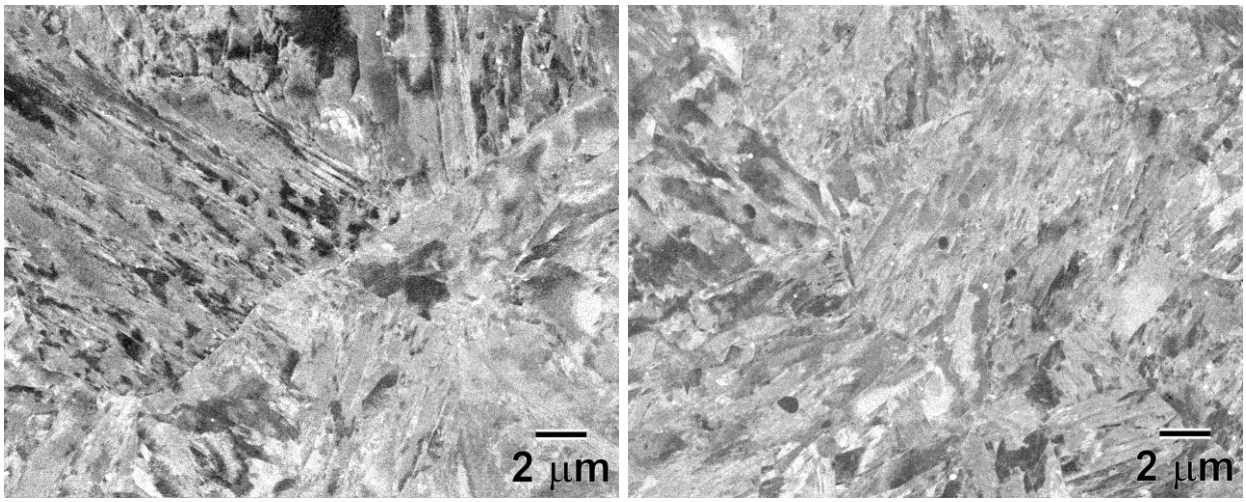

Figure 12. BSE micrographs showing the microstructure observed in the TMAZ of 9Cr FMS in sample 3A on (a) the ascending side and (b) the descending side.

the descending side (Fig. 12b). These observations suggest that the microstructure in the TMAZ reached temperatures far exceeding ~850ºC in order to cause complete austenization and dissolution of carbides in the microstructure followed by formation of martensite laths and precipitation of carbides upon cooling after passage of the rotating pin tool.

The interface region observed between the SZ and TMAZ of 14YWT on the ascending and descending sides of sample 1A is shown in Figure 13. The microstructure on the ascending side (Fig. 13a) experienced significant grain size coarsening in the SZ compared to that observed in the adjacent TMAZ. Most of the grains are larger than 5 μm in size, which represents an increase by a factor of up to 5-10X compared to the grain size observed in the unaffected zone (Fig. 8). The grain size also increased on the descending side of the SZ (Fig. 13b), but the increase was much less.

Figure 14 shows the microstructure of 14YWT that was observed at high magnification in the TMAZ and SZ of sample 1A. In the TMAZ (Fig. 14a), the size and morphology of the grains have been altered compared to the unaffected zone (Fig. 8b). Compared to the elongated grain morphology observed lying parallel to the extrusion direction, the grains in the TMAZ are nearly equiaxed with an increase in size to ~1 μm. The grains observed in the SZ (Fig. 14b) are also nearly equiaxed, but have undergone extensive coarsening. In addition, a relatively high number density of particles showing dark contrast relative to surrounding grains is observed in the large grains. The particle size resolved in the BSE micrographs is within the range from ~50 nm to ~350 nm. The preliminary composition analysis obtained by X-ray Energy Dispersive Spectroscopy (XEDS) showed that many of the dark contrast particles contained Ti and Y, but further analysis is still in progress. These results indicate that very high temperatures were reached in the SZ during passage of the rotating pin tool since significant increases in grain size and Y-, Ti-, O-enriched nanoclusters occurred in a relatively short period of time. The mechanism accounting for these rapid increases in size more likely was dynamic recrystallization.

(a) (b)

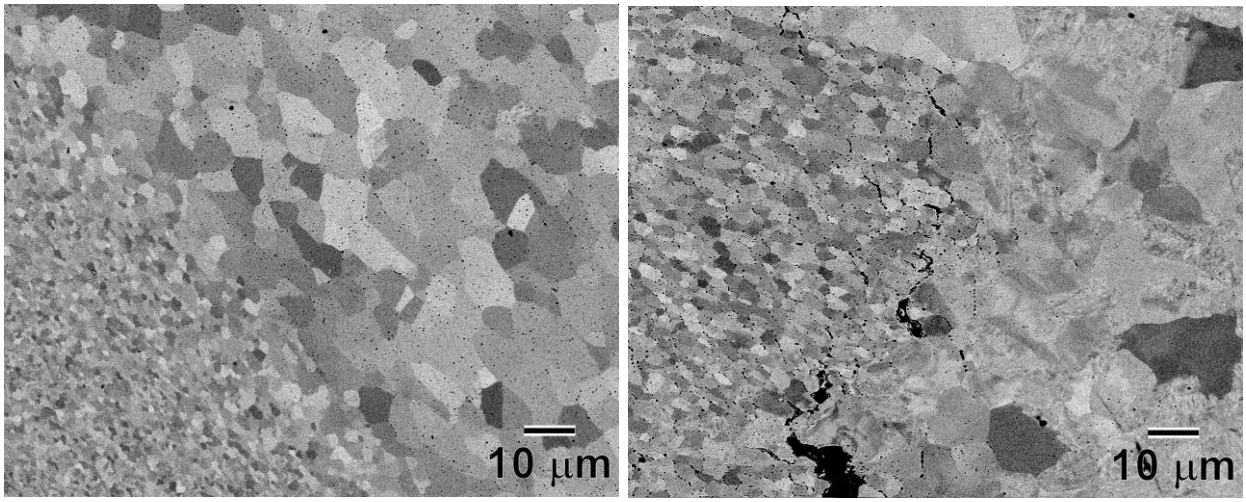

Figure 13. BSE micrographs showing the interface region observed between the SZ and TMAZ of 14YWT in sample 1A on (a) the ascending side and (b) the descending side.

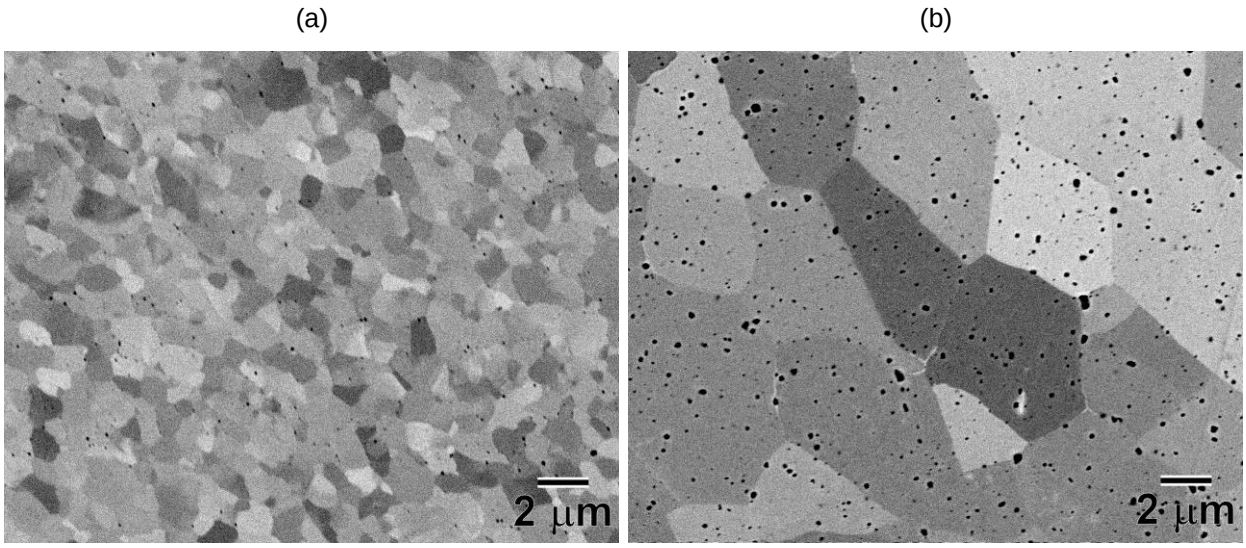

Figure 14. BSE micrographs showing the grain structure of 14YWT observed on the ascending side of sample 1A at high magnification in the (a) TMAZ and (b) SZ.

Conclusion

Friction stir welding was used to form a butt joint along an effective angle of 9.6º between 5 mm thick plates of ODS 14YWT and 9Cr FMS. Three cross section samples were cut from the joined plates representing solid-state mixtures of ~80%/20%, ~50%/50% and ~20%/80% by volume fraction of 14YWT and 9Cr FMS, respectively and prepared by metallographic procedures. The microstructural analysis of the SZ of the 3 samples by SEM showed no macro-scale pores formed. Only the ~50%/50% sample showed complete mixing between 14YWT and 9Cr FMS. The other two samples prepared from each end of the joined plates showed mixing between the two alloys only occurred near the top surface region of the joined plates where additional heating was caused by the shoulder of the rotating pin tool. The results indicated that very high temperatures from frictional heat occurred in the SZ that caused significant increases (up to 10X factor) in grain size and oxide particle size for 14YWT and decreases in prior austenite grain size and martensite lath size with dissolution of carbides for 9Cr FMS.

Future Work

Additional FSW experiments are planned that will focus on modifying the parameters (pressure, pin tool rotation rate and travel speed) in order to reduce the peak temperature reached in the SZ caused by frictional heating from the rotating pin tool. In addition, two additional samples will be extracted from the joined plates of 14YWT and 9Cr FMS from the initial FSW run in locations at are closer to the 2A (center) to obtain an more optimum mixture in volume fraction of 14YWT and 9Cr FMS. These samples will be prepared using metallographic procedures and investigated with SEM.

References

[1] D.T. Hoelzer, K.A. Unocic, M.A. Sokolov and Z. Feng, Journal of Nuclear Materials, Vol. 442, (2013), pp. 529-534.
[2] N.J. Cunningham, Y. Wu, G.R. Odette, D.T. Hoelzer and S.A. Maloy, Fusion Reactor Materials Program, DOE/ER-0313/54-Volume 54, (2013), p. 15-26.